American Mineralogist, Volume 81, pages 852–863, 1996

The nature of diffraction effects from illite and illite-smectite consisting of interstratified trans-vacant and cis-vacant 2:1 layers: A semiquantitative technique for determination of layer-type content

VICTOR A. DRITS[1] AND DOUGLAS K. MCCARTY[2]

[1]Geological Institute of the Russian Academy of Science, Pyzevskij per. D.7, 109017 Moscow, Russia
[2]Department of Earth Sciences, Montana State University, Bozeman, Montana 59717, U.S.A.

ABSTRACT

Previous work has described the structural and diffraction criteria for distinguishing between tv-1*M*, cv-1*M*, and *m*-1*M* illite varieties, where tv-1*M* illite corresponds to a structure with trans vacant (tv) 2:1 layers, cv-1*M* illite consists of cis-vacant (cv) 2:1 layers, and *m*-1*M* illites consist of 2:1 layers with random distributions of octahedral cations over trans and cis sites within each layer. Detailed analysis of calculated and experimental X-ray diffraction (XRD) patterns from illites and mixed-layered illite-smectites (I/S) with a range of cis- and trans-vacant layer interstratification, and consideration of unit-cell parameters for pure tv-1*M* and cv-1*M*, provides insight into the nature of the diffraction effects from the interlayered structures with different types and contents of rotational stacking defects. Structural fragments of the $2M_1$ and $2M_2$ polytypes exist within 1*Md* structures in which rotational disorder is dominated by $n \cdot 120$ and $n \cdot 60°$, respectively. Such structural fragments constitute coherent-scattering domains and affect the peak positions of the diagnostic 11*l* reflections for rotationally disordered I/S and illites in different ways depending on the proportion of cis- and trans-vacant 2:1 layers.

Simple techniques that do not require computer programs were developed for the semiquantitative determination of the proportion of tv and cv 2:1 layers in I/S and illites where such layers are interstratified. These techniques may help to reveal the diversity of I/S and illite samples relating to the conditions of their formation and transformation.

INTRODUCTION

Until recently the structural characterization of nonswelling dioctahedral micas was restricted by difficulties in determining the details of their polytype modification (Środoń and Eberl 1984). One-layer illites and glauconite are subdivided, depending on their structural perfection, between the 1*M* polytype, which has no rotational layer disorder, and the 1*Md* polytype, which contains many noncoincident azimuthal layer orientations.

Description of illite-smectite (I/S) has been restricted to the determination of proportions of illite and smectite interlayers and the ordering pattern in their distribution (Reynolds and Hower 1970; Drits and Sakharov 1976; Reynolds 1980). Most researchers have assumed that in all dioctahedral micas and I/S, 2:1 layers have tv octahedra. This supposition is based on single-crystal X-ray structure refinements in which octahedral cations in 2:1 layers of the various polytypes of muscovite, paragonite, and margarite were shown to occupy only cis sites (Bailey 1984). Drits et al. (1984) considered the hypothetical structural models for one-layer illites in which 2:1 layers have different distributions of octahedral cations over available trans and cis sites. They described the main structural and diffraction features for the following four models: (1) tv-1*M* illite consisting of trans-vacant (tv) 2:1 layers, (2) cv-1*M* illite consisting of cis-vacant (cv) 2:1 layers, (3) *m*-1*M* illite consisting of 2:1 layers with random distributions of octahedral cations over trans and cis sites within each layer, and (4) tv-cv illite consisting of randomly interstratified tv and cv 2:1 layers, but each layer is uniformly tv or cv.

The possible existence of these structures among natural dioctahedral micaceous minerals was assumed by analogy with dioctahedral smectites, the actual structures of which may consist of 2:1 layers with different distributions of octahedral cations over trans and cis sites (Tsipursky and Drits 1984). The pure cv-1*M* illite was described by Zvyagin et al. (1985) and Drits et al. (1993), and a mixture of cv-1*M*, tv-1*M*, and tv-$2M_1$ by Reynolds and Thomson (1993) and Drits et al. (1993). Gavrilov and Tsipursky (1987) described 1*M* illite with an almost random distribution of Al cations over available trans and cis sites.

Reynolds (1993), McCarty and Reynolds (1995), and Drits et al. (1996) showed that in some I/S so-called "fundamental" illite particles are mixed-layer structures in which tv and cv 2:1 layers are randomly interstratified. Coexistence of tv and cv layers was established in a nonswelling illite sample from the Amethyst Vein System,

0003–004X/96/0708–0852$05.00

Creede Mining District, Colorado (Bookin, personal communication). This sample was initially described as 3*T* illite (Horton 1983) because of the similarity of X-ray diffraction (XRD) patterns corresponding to cv-1*M*, tv-cv, and 3*T* illite structures (Drits et al. 1993).

To estimate the proportions of tv and cv 2:1 layers in illite and I/S, Reynolds (1993), McCarty and Reynolds (1995), and Bookin (personal communication) calculated diffraction effects of different structural models and then compared them with experimental XRD patterns from natural samples. Computer programs were used for these calculations.

Using the same approach, Sakharov et al. (1990) studied a large collection of glauconite samples with different chemical compositions, ages, and degrees of structural perfection. They found that all the glauconite samples studied consisted of tv 2:1 layers. It seems likely, therefore, that coexistence of tv and cv 2:1 layers within the same particle or coherent-scattering domain is a characteristic feature of some illites and I/S, whereas the structure of glauconite is restricted to the tv type. The mechanism resulting in these respective structural differences is still under investigation.

Mica polytypes differ by azimuthal orientations of the successive 2:1 layers resulting from layer rotations by $n \cdot 120°$ (n is an integer) or $n \cdot 60°$ (n is an odd integer) around the axis normal to the (001) plane and passing through a K cation in mica interlayers. In pure 1*M* illite all layers have the same azimuthal orientation, whereas in $2M_1$ and $2M_2$ polytypes the azimuthal orientations of any adjacent layers differ by 120 or 60°, respectively. Three-dimensional periodicity of mica polytypes and, in particular, 1*M* illite may be completely or partially destroyed because of the presence of rotational stacking faults. For example, so-called semiordered 1*Md* micas may contain some stacking faults owing to layer rotations by ±120° or by $n \cdot 60°$ (Sakharov et al. 1990; Reynolds 1993; McCarty and Reynolds 1995).

The aim of this paper is to describe the nature of the diffraction effects from interstratified tv and cv 2:1 layers in illites and I/S that contain rotational stacking faults and to introduce techniques for semiquantitative estimation of layer-type content that do not require computer programs.

Method

Interstratification of tv and cv illite layers that have identical azimuthal orientation: Development of Méring's principles

Méring (1949) proposed a model that predicts general regularities in the observed diffraction effects from interstratified structures. Méring's first principle is that basal reflections for two-component random mixed-layer structures must be situated along the c^* axis in reciprocal space and between the most closely spaced 00*l* nodes corresponding to periodic structures with interstratified layers.

Méring's second principle is that basal node positions corresponding to the mixed-layer structure depend on the proportions of interstratified layers. This dependence can be expressed by a simple linear relationship,

$$W_A = \frac{y}{x + y} \quad (1)$$

where W_A is the layer proportion of type A, and x and y are the distances between nodes corresponding to the mixed-layer structure and the nearest l_A and l_B nodes corresponding to two periodic components. Thus, the XRD patterns from mixed-layer minerals differ from those of periodic clay minerals by the presence of a nonrational series of basal reflections. From the diffraction point of view the migration of a node corresponding to a mixed-layer structure results from the migration of the maximum of the interference function. For this reason the nature of diffraction effects observed for the structures that have disorder resulting from alternation of layers having different thicknesses should be analogous to that observed for the structures that have disorder resulting from interstratification of layers having the same thickness but different internal structures and interlayer displacements along the a direction. If this assumption is valid then Méring's principles can be applied to the non-basal reflections of a two-component mixed-layer structure that are situated between the most closely spaced *hkl* nodes corresponding to the pure minerals that make up the interstratified mixture.

Figure 1 shows XRD curves, excluding basal reflections, calculated for tv-1*M* and cv-1*M* illites according

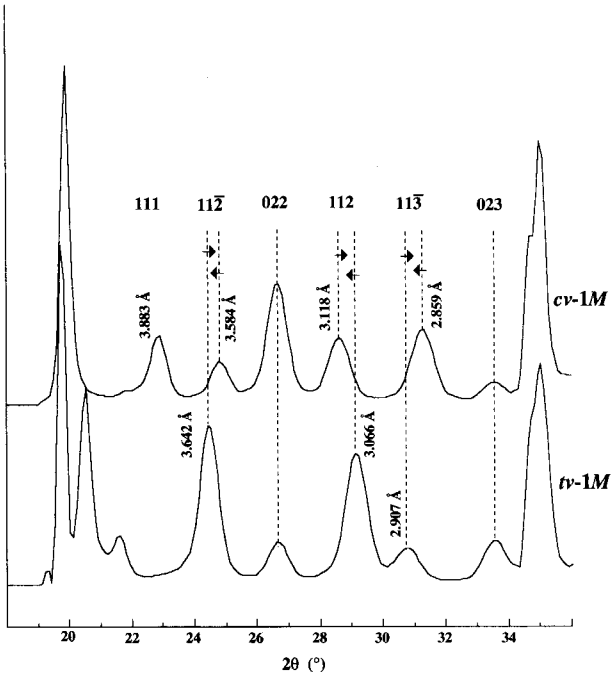

FIGURE 1. Calculated diffraction patterns corresponding to tv-1*M* and cv-1*M* illites. Notice that the positions of reflections that have the same indices do not coincide.

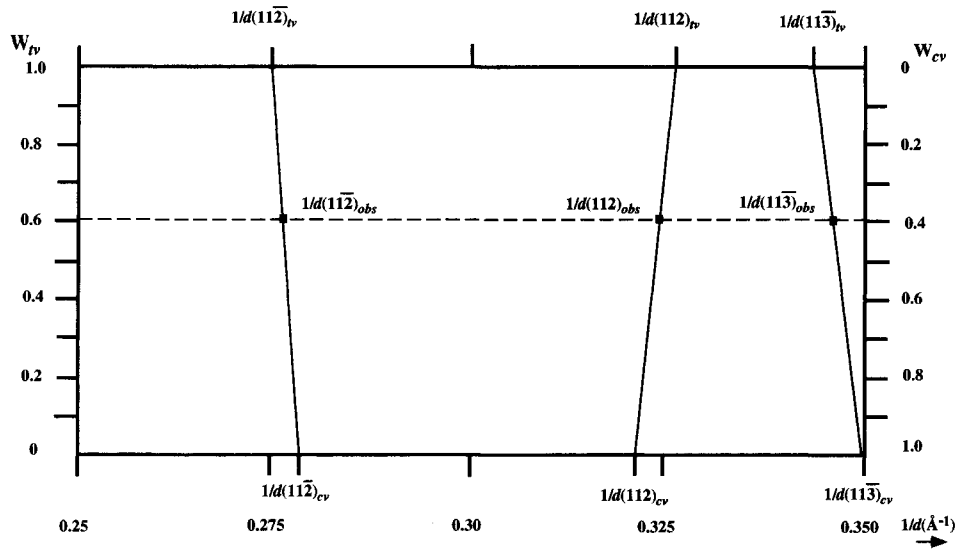

FIGURE 2. The nearest neighbor reciprocal lattice nodes for tv-1*M* and cv-1*M* illites that have the same *hkl* indices. In the rectangle, the points corresponding to each such pair of nodes are joined by lines that reflect the migration of the nodes corresponding to tv-cv illites as a result of Méring's principles.

to the technique described by Drits et al. (1984) (where the number of layers, *N*, equals 10). The presence of two strong reflections that have indices $11\bar{2}$ and 112 is the characteristic feature of the XRD patterns from tv-1*M* illites. The XRD curve for cv-1*M* illites contains four reflections that have indices 111, $11\bar{2}$, 112, and $11\bar{3}$ and similar intensities in addition to the strong 022 reflection, the position of which practically coincides with the 003 reflection.

Figure 1 shows that the positions of reflections that have the same indices in tv-1*M* and cv-1*M* illites do not coincide. The main reason is that different structural distortion of tv and cv layers leads to a particular relationship between the unit-cell parameters of tv-1*M* and cv-1*M* illites. The electrostatic forces in the basic mica structure distort tv and cv layers in different ways (Drits et al. 1984). In general, the *a* and *b* unit-cell dimensions in both cv and tv layers are nearly equal, but the unit-cell parameter *c* and the β angle differ significantly. For example, in both cv and tv-1*M* structures described by Drits et al. (1984) $a = 5.199$, $b = 9.005$, but $c = 10.09$ Å and $\beta = 99.13°$ in the cv structure and $c = 10.164$ Å and $\beta = 101.3°$ in the tv structure (Tsipursky and Drits 1984; Drits et al. 1984). These differences in the unit-cell parameters result in differences in the values of the relationship $|(c \cos \beta)/a|$ for pure tv-1*M* and cv-1*M* structures (Drits et al. 1984, 1993). The different values of this parameter reflect the different relative displacements along the *a* axis of one 2:1 layer with respect to the preceding layer in these two structural modifications.

Following Méring's principles we can predict the diffraction effects for tv-cv illites. Because the projections of tv-1*M* and cv-1*M* structures coincide along the *a* direction of their unit cells, the waves scattered in the directions of the 02*l* reflections are in phase. For this reason positions of the 02*l* reflections corresponding to tv-cv illites do not depend on the proportions of tv and cv layers. Therefore, only the behavior of the $11l, 11\bar{l}$ reflections, which are most sensitive to the content of the layer types, needs to be considered.

Let us designate 11*l* indices corresponding to tv-1*M* and cv-1*M* illites as $11l_{tv}$ and $11l_{cv}$, respectively. Figure 1 shows that the $11\bar{2}_{tv}$, 112_{tv}, and $11\bar{3}_{tv}$ reflections should migrate, respectively, toward the $11\bar{2}_{cv}$, 112_{cv}, and $11\bar{3}_{cv}$ reflections with a successive decrease of tv 2:1 layer proportions from 1 to 0.

The lower side of the rectangle shown in Figure 2 contains the $11l, 11\bar{l}$ nodes of the reciprocal lattice of cv-1*M* illite, and the upper side is the same scale and contains the $11l, 11\bar{l}$ nodes of the reciprocal lattice of tv-1*M* illite. On the left vertical side the numbers correspond to tv 2:1 layer content from 1.0 at the top to 0 at the bottom, and on the right vertical side the numbers correspond to cv-layer content from 1.0 at the bottom to 0 at the top. The positions of the $11l, 11\bar{l}$ nodes on the upper and lower sides correspond to $1/d(11l, 11\bar{l})_{tv}$ and $1/d(11l, 11\bar{l})_{cv}$, respectively. The spacings of the $(11l, 11\bar{l})_{tv}$ and $(11l, 11\bar{l})_{cv}$ reflections can be determined from the XRD patterns and predicted from the unit-cell parameters corresponding, respectively, to tv-1*M* and cv-1*M* illites (Drits et al. 1993).

In Figure 2 the nearest neighboring reciprocal lattice nodes for tv-1*M* and cv-1*M* illites have the same *hkl* indices. In the rectangle, the points corresponding to each such pair of nodes are joined by solid lines. These migration lines reflect the migration of the nodes corresponding to tv-cv illites. Diffraction nodes for every definite proportion of tv 2:1 layers (W_{tv}) occur at points where the horizontal lines joining W_{tv} and $W_{cv} = 1 - W_{tv}$ (the right side of the rectangle) intersect with inclined solid lines connected to the reciprocal lattice nodes of the periodic components.

Proportions of tv and cv layers can be determined by

using the graphical technique or calculated with the help of linear relationships similar to Equation 1. Figure 2 indicates that the following equations for determining the W_{cv} values can be obtained:

$$W_{cv} = \frac{1/d_{11\bar{2}_{obs}} - 1/d_{11\bar{2}_{tv}}}{1/d_{11\bar{2}_{cv}} - d_{11\bar{2}_{tv}}} = \frac{1/d_{112_{tv}} - 1/d_{112_{obs}}}{1/d_{112_{tv}} - 1/d_{112_{cv}}}$$

$$= \frac{1/d_{11\bar{3}_{obs}} - 1/d_{11\bar{3}_{tv}}}{1/d_{11\bar{3}_{cv}} - 1/d_{11\bar{3}_{tv}}}. \quad (2)$$

Here $d(11l,11\bar{l})_{obs}$ is the spacing of the $11l$ reflection corresponding to tv-cv illite, which is situated between the nodes of tv-1M and cv-1M illites that have the same $11l$ indices.

Determination of W_{cv} for pure tv-1M and cv-1M illites

Another way to determine the proportion of cv layers, W_{cv}, is by measuring the d values of the diagnostic $11l,11\bar{l}$ reflections. If $T = |(c \cos \beta)/a|$, then using the relationship between the parameters of a monoclinic unit cell and $d(hkl)$ values, the following equations can be obtained:

$$T = \frac{c \cos \beta}{a} = 0.125(c \sin \beta)^2\left[\frac{1}{d^2_{11\bar{2}}} - \frac{1}{d^2_{112}}\right]$$

$$= 0.125(c \sin \beta)^2\left[\frac{1}{d^2_{11\bar{3}}} - \frac{1}{d^2_{111}}\right] - 1$$

$$= 0.1(c \sin \beta)^2\left[\frac{1}{d^2_{11\bar{3}}} - \frac{1}{d^2_{112}}\right] - 0.5. \quad (3)$$

Equation 3 permits calculation of the T values for pure cv-1M and tv-1M as well as for tv-cv illites if $d(001) = c \sin \beta$ and the $d(11l,11\bar{l})$ values are determined from the reflections recorded in experimental or calculated XRD patterns. As mentioned, the $T = |(c \cos \beta)/a|$ parameter has different values for tv-1M and cv-1M illites. One may assume that in cases of random interstratification of tv and cv 2:1 layers, the effective value of the parameter, $T_{ef} = |(c \cos \beta)/a|$, should be a statistically weighted sum of the $T_{tv} = |(c \cos \beta)/a|_{tv}$ and $T_{cv} = |(c \cos \beta)/a|_{cv}$ values corresponding to tv-1M and cv-1M illites. The weight for the T_{tv} and T_{cv} terms should be proportional to the content of tv and cv 2:1 layers. The consequence of this assumption is the following:

$$T_{ef} = W_{tv}T_{tv} + W_{cv}T_{cv} = T_{tv} - W_{cv}(T_{tv} - T_{cv})$$

or

$$W_{cv} = \frac{T_{tv} - T_{ef}}{T_{tv} - T_{cv}}. \quad (4)$$

Thus, to use this technique one has to measure the angular positions for $11l,11\bar{l}$ reflections in XRD patterns from tv-cv illites, calculate the $d(11l,11\bar{l})$ and T_{ef} values, and then use Equation 4 to estimate the W_{cv} value. Analysis of XRD patterns from pure tv-1M and cv-1M illites containing a small amount of Fe (unit-cell parameter $b \leq 9.01$ Å) has shown that the T_{tv} and T_{cv} values are equal to 0.400 and 0.302, respectively (Drits et al 1993). The

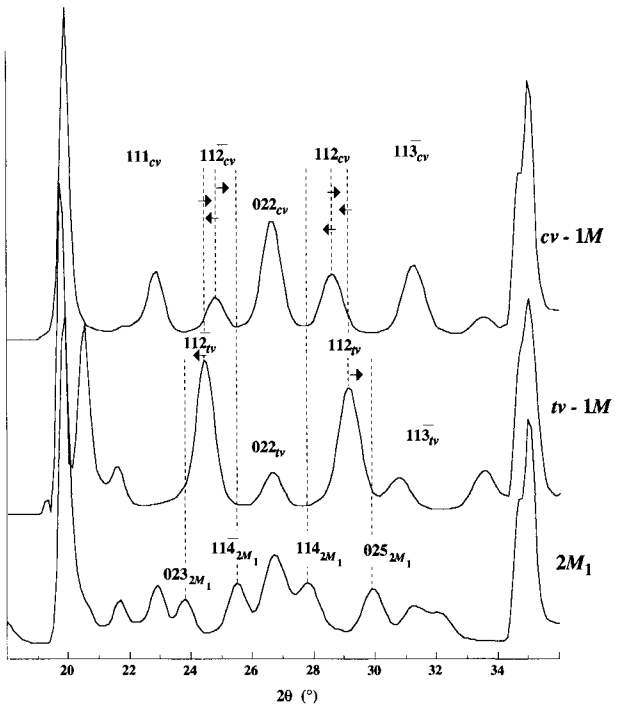

FIGURE 3. Disposition of the $0kl$ and $11l$ reflections in XRD powder patterns corresponding to periodic tv-1M, cv-1M, and tv-2M_1 modifications. The presence of stacking faults by $n \cdot 120°$ introduces fragments of the $2M_1$ polytype to the basic 1M structure and as a result leads to new diffraction effects determined by an "interaction" of the $11l,0kl$ reflections for each structure that is controlled by the proportion of layer types, the fixed content of cv 2:1 layers, and the proportions of stacking faults.

β angle and c parameter determined for tv-cv illites must be considered as apparent because they have no real physical meaning.

tv-cv illites containing rotational stacking faults

In structures with rotational disorder (1Md) there are fundamental crystallographic and diffraction differences between $n \cdot 120°$ (n = integer) and $n \cdot 60°$ (n = odd integer) disorder (McCarty and Reynolds 1995). In structures with $n \cdot 120°$ disorder there are thin fragments of the $2M_1$ polytype, with either cv or tv layers, that constitute coherent-scattering domains (CSD) and interfere with the 1M reflections. Similarly, structures with $n \cdot 60°$ disorder have fragments of the $2M_2$ polytype constituting CSDs. The tv-$2M_1$ and cv-$2M_1$, or tv-$2M_2$ and cv-$2M_2$ fragments appear because of the random formation of pairs, triplets, or larger combinations consisting of tv or cv 2:1 layers that are stacked as in the regular $2M_1$ or $2M_2$ mica polytype. Méring's approach explains the displacement of the 1M reflections, which affect the precision of the W_{cv} values obtained from Equations 2 and 4. For example, see Figures 3 and 4 for the effects of the $2M_1$ and $2M_2$ maxima on the positions of the 1M $11\bar{2}$ peak for both cv and tv structures. The total diffraction effects depend on the proportions of the cv and tv layers and the type and quantity of stacking faults. Table 1 summarizes the dif-

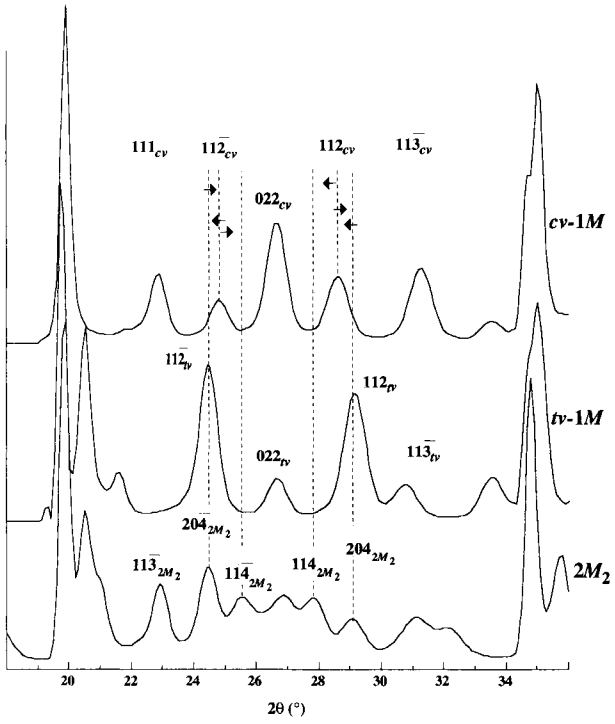

FIGURE 4. Disposition of the $0kl$ and $11l$ reflections in XRD powder patterns corresponding to periodic tv-1M, cv-1M, and tv-2M_2 modifications. The presence of stacking faults by $n\cdot60°$ introduces fragments of the $2M_2$ polytype to the basic 1M structure and as a result leads to new diffraction effects determined by an "interaction" of the $11l,0kl$ reflections for each structure that is controlled by the proportion of layer types, the fixed content of cv 2:1 layers, and the proportions of stacking faults.

fraction effects for relative cv- and tv-layer content and the type and amounts of rotational disorder.

RESULTS

Comparison of the actual and calculated W_{cv} values

To check the validity of our assumptions concerning the nature of the diffraction effects in illite and I/S, and to estimate the effectiveness of the techniques proposed, we analyzed XRD patterns simulated for tv-cv I/S structural models differing by the proportion of layer type and by the nature and amount of layer rotations. The main aim was to determine the discrepancy between the actual proportions of tv and cv layers in tv-cv illites, containing different contents of rotational stacking faults, and the W_{cv} values calculated using the techniques proposed. The WILDFIRE computer program (Reynolds 1993) was used for simulation of the XRD patterns. Atomic coordinates and unit-cell parameters for the tv-1M and cv-1M illite structures used for the calculations are from Drits et al. (1984). Both unit cells have the same lengths, $a = 5.199$, $b = 9.005$, $c \sin\beta = 9.98$ Å, but different $T = |(c\cos\beta)/a|$ values ($T_{tv} = -0.383$ and $T_{cv} = -0.308$). To describe the tv-cv illite structural models, a set of variable parameters were used (McCarty and Reynolds 1995). P_0 is the proportion of layers rotated zero degrees with respect to the preceding layer. P_{60} is the proportion of layers rotated 60, 180, and 300°. $P_r = 1 - P_0$ is the fraction of non-coincident adjacent layers, and P_{60} is also the fraction of P_r that consists of equal proportions of 60, 180, and 300° rotations. Therefore, $P_{60} = 0$ shows that the structural disorder is due to layer rotations by ±120°, and $P_{60} = 1$ indicates that all the structural disorder is of the type $n\cdot60°$ (n = odd integer). For example, in a structure with $P_0 = 0.55$ and $P_{60} = 0.6$, there is an equal probability of 60, 120, 180, 240, and 300° rotations, each of which is equal to 0.09. For all tv-cv illite models the number of unit cells within the CSD, N_3, was equal to 10. Let us call the actual cv-layer content used in WILDFIRE P_{cv} and the cv-layer content calculated using Equations 2 and 4 W_{cv}. Then $W_{cv} + W_{tv} = 1$ and $P_{cv} + P_{tv} = 1$.

TABLE 1. Effect on calculated content of cv 2:1 layers, W_{cv}, in tv-cv illites with $n\cdot60°$ (n = odd integer) and ±120° disorder

Condition	Effects on calculated W_{cv} from Eqs. 2 and 4
$W_{tv} > W_{cv}$ and ±120° layer rotations	Underestimated
$W_{cv} > W_{tv}$ and ±120° layer rotations	Overestimated
$W_{tv} > W_{cv}$ and $n\cdot60°$ layer rotations	Underestimated
$W_{cv} > W_{tv}$ and $n\cdot60°$ layer rotations	Overestimated

Note: For a given content of rotational stacking faults and $W_{tv} > W_{cv}$, the difference between the actual and calculated W_{cv} values for structures containing $n\cdot60°$ rotations is smaller than that for the structures containing ±120° rotations. For tv-cv illites having $W_{cv} > W_{tv}$, the difference between the compared values should be approximately the same regardless of the nature of layer rotations.

Figures 5–7 show some of the simulated XRD curves, and Table 2 contains the $d(11l,11\bar{l})_{obs}$ values determined from the XRD patterns corresponding to the tv-cv models with different P_{cv}, P_0, and P_{60} values. The analysis of the simulated XRD patterns has shown that the techniques proposed cannot be used for tv-cv illites with $P_0 < 0.6$ and $P_{60} = 0$ or $P_0 < 0.5$ and $P_{60} = 1$. The XRD patterns with these P_0 and P_{60} values contain very weak and broad reflections, the positions of which cannot be precisely determined (Figs. 6 and 7).

Determination of W_{cv} values for tv-cv illites that have the same layer orientation

Méring's approach. Table 2 compares P_{cv} values with the $d(11l,11\bar{l})_{obs}$ values for the models with $P_0 = 0.5$ to 1 and $P_{60} = 0$ and 1. The mean value, $\overline{W}_{cv}$, of the W_{cv} values obtained from Equation 2, corresponding to the spacings of the $11\bar{2}_{obs}$, 112_{obs}, and $11\bar{3}_{obs}$ reflections for each simulated pattern, is given in Table 3. The absolute values of P_{cv} and $\overline{W}_{cv}$ differ by only 0.02–0.04. It should be noted that the same differences are observed between P_{cv} and W_{cv} calculated using $d(112)_{obs}$ values (Table 3). Divergence between P_{cv} and W_{cv} calculated using $d(11\bar{2})_{obs}$ and $d(11\bar{3})_{obs}$ values does not exceed 0.06 (Table 3). The main reason for the difference in conformity between P_{cv} and W_{cv} calculated using different values of $d(11l,11\bar{l})_{obs}$

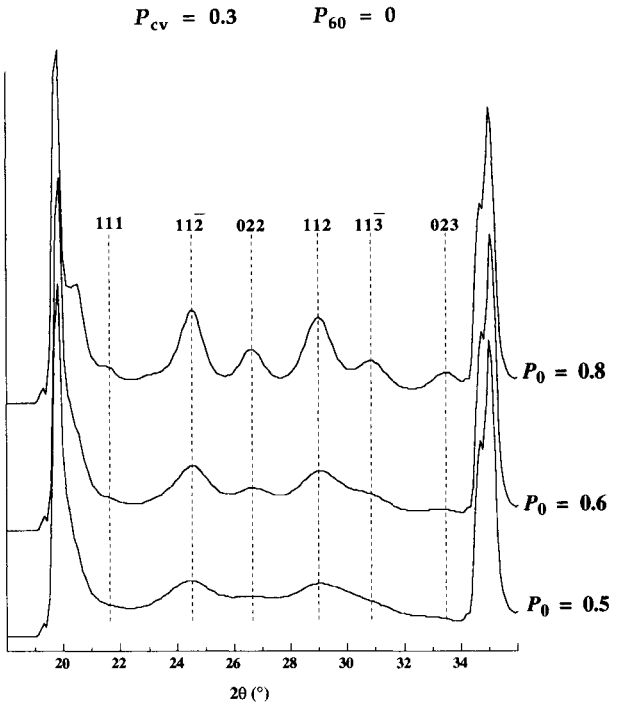

FIGURE 5. Calculated XRD curves showing the diffraction effects that the type and amount of rotational stacking faults have on the 11*l*,02*l* reflections used to determine W_{cv}. P_{cv} = 0.3, rotations are all $n \cdot 120°$, and P_0 = 0.8, 0.6, and 0.5.

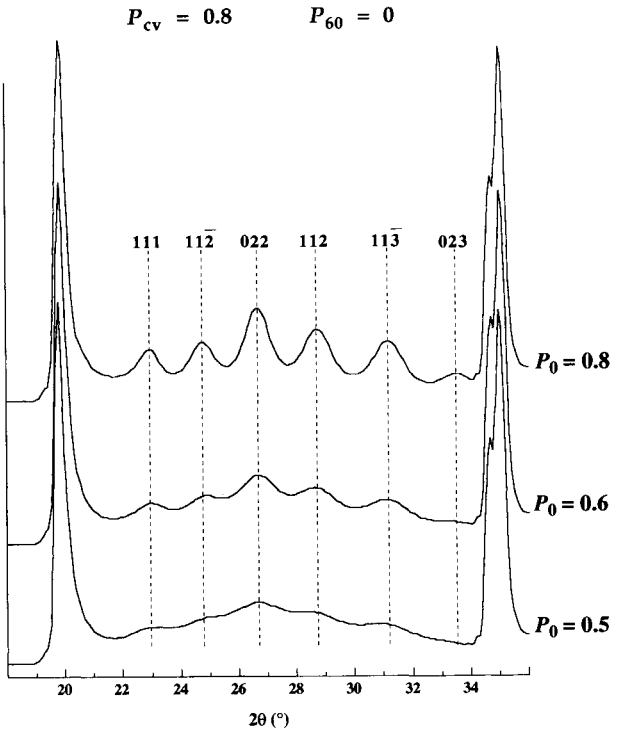

FIGURE 6. Calculated XRD curves showing the diffraction effects that the type and amount of rotational stacking faults have on the 11*l*,02*l* reflections used to determine W_{cv}. P_{cv} = 0.8, rotations are all $n \cdot 120°$, and P_0 = 0.8, 0.6, and 0.5.

is that the difference in intensities between the 112_{tv} and 112_{cv} reflections is smaller than that for the other two pairs of reflections (Fig. 1).

Utilization of the T_{ef} values. For each given P_{cv} value, two values of T_{ef} were calculated using Equation 3 and the values for $d(112)_{obs}$, $d(11\bar{3})_{obs}$ and for $d(112)_{obs}$, $d(11\bar{2})_{obs}$ shown in Table 2. Table 4 compares the P_{cv} values with those calculated using the spacings from different pairs of reflections. The difference between compared values is much smaller when the spacings from the 112_{obs} and $11\bar{3}_{obs}$ reflections are used. For each given P_{cv}, the mean of the two calculated W_{cv} values, $\overline{W}_{cv}$, is also given in Table 4. The differences between P_{cv} and $\overline{W}_{cv}$ do not exceed 0.04. Thus, the techniques proposed may be applied for fast, simple, and quantitative determination if tv-cv illite samples do not contain rotational stacking faults. The presence of stacking faults is simply determined by visual inspection of the diffraction pattern. Rotational stacking faults broaden the 11*l* and 02*l* peaks a great deal but do not broaden the 20*l*,20$\bar{l}$ and 13*l*,13$\bar{l}$ peaks significantly. This type of selective peak broadening can be distinguished from peak broadening caused by small CSD due to thin crystals, which broadens all the peaks in the diffraction pattern. If the 11*l*,11$\bar{l}$ peaks in the experimental diffraction pattern are distinct and well resolved, then the $d(11l)_{obs}$ and $d(11\bar{l})_{obs}$ values can be measured and the cv and tv contents successfully calculated using this method.

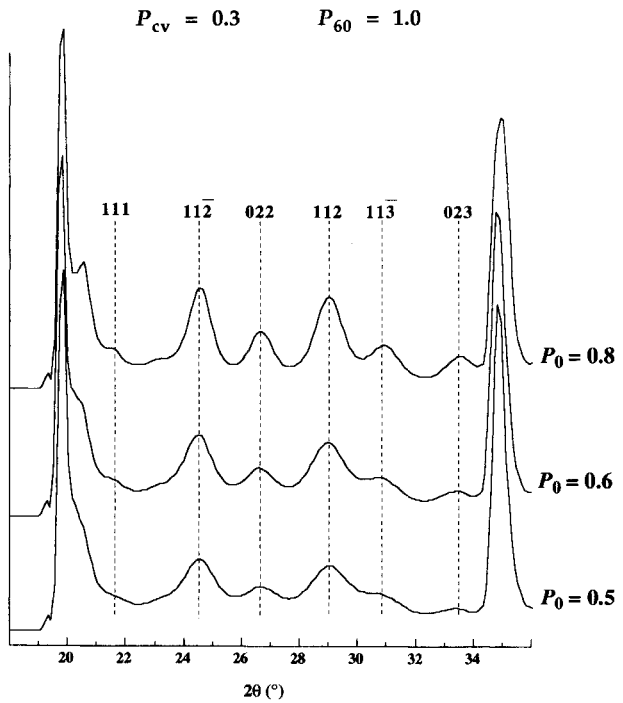

FIGURE 7. Calculated XRD curves showing the diffraction effects that the type and amount of rotational stacking faults have on the 11*l*,02*l* reflections used to determine W_{cv}. P_{cv} = 0.3, rotations are all $n \cdot 60°$, and P_0 = 0.8, 0.6, and 0.5.

TABLE 2. The d values from calculated diffraction patterns with rotations of $n \cdot 120$ and $n \cdot 60°$ in comparison with d values for pure tv and cv unit cells

Calculated pattern P_{cv}	P_0	$d(111)$ $P_{60} = 0$	$d(111)$ $P_{60} = 1.0$	$d(11\bar{2})$ $P_{60} = 0$	$d(11\bar{2})$ $P_{60} = 1.0$	$d(112)$ $P_{60} = 0$	$d(112)$ $P_{60} = 1.0$	$d(11\bar{3})$ $P_{60} = 0$	$d(11\bar{3})$ $P_{60} = 1.0$
0	1.0			3.642	3.642	3.066	3.066	2.907	2.907
0	0.8			3.642	3.642	3.063	3.064	2.919	
0	0.6			3.648	3.647	3.056	3.063		
0	0.5			3.656	3.647	3.043	3.062		
0.2	1.0			3.633	3.633	3.076	3.076	2.897	2.897
0.2	0.8			3.634	3.633	3.075	3.076	2.905	2.902
0.2	0.6			3.641	3.638	3.068	3.076		
0.2	0.5			3.645	3.638	3.064	3.072		
0.3	1.0	3.867	3.867	3.629	3.629	3.081	3.081	2.890	2.890
0.3	0.8			3.629	3.629	3.080	3.082	2.897	2.896
0.3	0.6			3.630	3.633	3.076	3.079		2.905
0.3	0.5			3.638	3.633	3.069	3.079		
0.4	1.0	3.870	3.870	3.620	3.620	3.085	3.090	2.888	2.888
0.4	0.8			3.625	3.625	3.086	3.085	2.892	2.880
0.4	0.6			3.626	3.625	3.085	3.085	2.905	2.899
0.4	0.5			3.626	3.629	3.080	3.085		2.909
0.5	1.0	3.872	3.872	3.617	3.617	3.089	3.089	2.884	2.884
0.5	0.8	3.856	3.861	3.620	3.625	3.088	3.089	2.886	2.887
0.5	0.6		3.851	3.620	3.622	3.089	3.092	2.890	2.891
0.5	0.5			3.617	3.620	3.090	3.092		2.899
0.6	1.0	3.870	3.870	3.613	3.613	3.096	3.096	2.880	2.880
0.6	0.8	3.875	3.872	3.613	3.614	3.098	3.097	2.882	2.880
0.6	0.6		3.867	3.609	3.615	3.099	3.099	2.900	2.885
0.6	0.5		3.851	3.604	3.611	3.102	3.098		2.888
0.8	1.0	3.870	3.870	3.597	3.597	3.107	3.107	2.868	2.868
0.8	0.8	3.882	3.882	3.597	3.601	3.107	3.108	2.873	2.871
0.8	0.6	3.875	3.882	3.584	3.597	3.121	3.112	2.879	2.873
0.8	0.5		3.877		3.593		3.115		2.880
1.0	1.0	3.883	3.883	3.584	3.589	3.118	3.118	2.859	2.859
1.0	0.8	3.882	3.888	3.579	3.584	3.123	3.118	2.862	2.860
1.0	0.6	3.883	3.890		3.570	3.144	3.125	2.862	2.862
1.0	0.5	3.882	3.888		3.558		3.135	2.870	2.862

Determination of W_{cv} values for tv-cv illites containing rotational stacking faults

Méring's approach. Table 5 contains the W_{cv} values calculated for tv-cv illites that have different P_{cv}, P_0, and P_{60} values. Calculations used Equation 2 and the $d(11\bar{2})_{obs}$ and $d(112)_{obs}$ values given in Table 2. For each given value of P_{cv}, P_0, and P_{60}, the mean of the two calculated W_{cv} values, $\overline{W}_{cv}$, is also given in Table 5. The data obtained confirm the main regularities, which are predicted in accordance with the utilization of Méring's principles for tv-cv illites containing rotational stacking faults. Let us note some of them for tv-cv illites with $P_{cv} < 0.5$ and $P_0 < 1.0$ (Table 5). For a given P_0, the W_{cv} values are lower than P_{cv} values. For each given $P_{cv} \leq 0.4$, the W_{cv} values decrease with decreasing P_0. As a result, the difference between P_{cv} and W_{cv} increases with decreasing P_0. For tv-cv illites with $0.3 \leq P_{cv} \leq 0.5$, the P_{cv} values can exceed the W_{cv} up to 0.10 if $P_0 \leq 0.6$ (Table 5). The difference between P_{cv} and $\overline{W}_{cv}$ exceeds 0.10 only for tv-cv illites with $0.2 \geq P_{cv} \geq 0$, $P_{60} = 0$, and $P_0 \leq 0.6$. Negative values of W_{cv} for tv-1M illites with $P_0 \leq 0.8$ and $P_{60} = 0$ reflect the influence of the presence of $2M_1$ structural fragments on the positions of $11\bar{2}_{obs}$ and 112_{obs} reflections. As expected, if $P_{60} = 1$, W_{cv} values are obtained only for tv-cv illites with $P_0 \geq 0.5$. If a negative value is obtained using Equation 2, it means there are no cv layers, but there are rotational stacking faults in the structure.

For tv-cv illites with $P_{cv} \geq 0.5$ and $P_0 < 1$, the follow-

TABLE 3. W_{cv} values for tv-cv illites without stacking faults, calculated using Equation 2 and the indicated $d(hkl)$ reflection

P_{cv}	W_{cv} $d(11\bar{2})_{obs}$	W_{cv} $d(112)_{obs}$	W_{cv} $d(11\bar{3})_{obs}$	$\overline{W}_{cv}$ Mean value
0.2	0.17	0.20	0.21	0.19
0.3	0.24	0.29	0.36	0.30
0.4	0.41	0.37	0.39	0.39
0.5	0.47	0.45	0.47	0.46
0.6	0.54	0.58	0.58	0.57
0.8	0.85	0.79	0.81	0.82

Note: P_{cv} is actual cv-layer content used in WILDFIRE.

TABLE 4. W_{cv} values for tv-cv illites without stacking faults, calculated using Equation 4 and the indicated $d(hkl)$ reflection pairs

P_{cv}	W_{cv} 112, 11$\bar{3}$	W_{cv} 11$\bar{2}$, 112	$\overline{W}_{cv}$ Mean value
0	0.02	−0.03	−0.01
0.2	0.22	0.16	0.19
0.3	0.35	0.24	0.30
0.4	0.41	0.32	0.37
0.5	0.49	0.42	0.46
0.6	0.61	0.54	0.58
0.8	0.89	0.75	0.82
1.0	1.01	0.93	0.97

TABLE 5. W_{cv} values for tv-cv illites containing $n \cdot 120°$ ($P_{60} = 0$) and $n \cdot 60°$ ($P_{60} = 1$) layer rotations, calculated using Equation 2 and the indicated $d(hkl)$ reflections

P_{cv}	P_0	W_{cv} $11\bar{2}_{obs}$ $P_{60} = 0$	W_{cv} 112_{obs} $P_{60} = 0$	$\overline{W}_{cv}$ $P_{60} = 0$	W_{cv} $11\bar{2}_{obs}$ $P_{60} = 1$	W_{cv} 112_{obs} $P_{60} = 1$	$\overline{W}_{cv}$ $P_{60} = 1$
0	0.8	0	−0.06	−0.03	0	−0.04	−0.02
0	0.6	−0.11	−0.20	−0.15	−0.09	−0.06	−0.07
0	0.5	—	—	—	−0.09	−0.08	−0.08
0.2	0.8	0.15	0.18	0.17	0.17	0.20	0.19
0.2	0.6	0.02	0.04	0.03	0.07	0.20	0.14
0.2	0.5	—	—	—	0.07	0.12	0.10
0.3	0.8	0.24	0.27	0.25	0.24	0.31	0.28
0.3	0.6	0.22	0.21	0.21	0.17	0.25	0.21
0.3	0.5	—	—	—	0.17	0.25	0.21
0.4	0.8	0.32	0.39	0.36	0.32	0.37	0.35
0.4	0.6	0.30	0.37	0.34	0.32	0.37	0.35
0.4	0.5	0.30	0.27	0.29	0.24	0.37	0.30
0.5	0.8	0.41	0.43	0.42	0.32	0.45	0.39
0.5	0.6	0.41	0.45	0.43	0.37	0.50	0.44
0.5	0.5	0.47	0.47	0.47	0.41	0.50	0.46
0.6	0.8	0.50	0.62	0.56	0.52	0.60	0.56
0.6	0.6	0.62	0.64	0.63	0.50	0.64	0.57
0.6	0.5	0.71	0.70	0.71	0.58	0.62	0.60
0.8	0.8	0.85	0.79	0.82	0.77	0.81	0.79
0.8	0.6	1.09	1.06	1.07	0.85	1.08	0.96
0.8	0.5	—	—	—	0.92	1.13	1.02
1.0	0.8	1.19	1.09	1.14	1.09	1.00	1.04
1.0	0.6	≫1.0	≫1.0	≫1.0	1.36	1.11	1.23

ing relationship between P_{cv} and W_{cv} was observed (Table 5). For each given P_{cv}, the W_{cv} values increase with decreasing values of P_0. The differences between P_{cv} and W_{cv} do not exceed 0.1 for tv-cv illites with $P_{cv} \geq 0.8$ and $P_0 > 0.7$. The W_{cv} values corresponding to tv-cv illites with $P_{cv} \geq 0.8$ and $P_0 \leq 0.6$ exceed 1.0. These results indicate the influence of stacking faults on the positions of the $11\bar{2}_{obs}$ and 112_{obs} reflections. Thus, if W_{cv} obtained from Equation 2 is >1, only cv layers are present and the structure contains rotational stacking faults. As in the case of tv-cv illites with the same layer orientation, the agreement between P_{cv} and W_{cv} is better when W_{cv} is determined using spacings from the 112 reflection.

Utilization of the T_{ef} values. T_{ef} values were calculated using Equation 3 and the $d(11l,11\bar{l})_{obs}$ values given in Table 2. The data obtained were used in Equation 4 to determine the W_{cv} values. Table 5 compares the P_{cv} values with those determined for tv-cv illites that have different P_0 values and P_{60} equal either to 0 or 1. The data given in Table 5 show that the technique proposed may be effectively used for semiquantitative determination of W_{cv} for tv-cv illites with $P_{cv} \geq 0.3$, $P_0 \geq 0.6$, and $P_{60} = 0$ or $P_{cv} \geq 0.2$, $P_0 \geq 0.5$, and $P_{60} = 1$. For these structural models maximal errors in $\overline{W}_{cv}$ do not exceed 0.10. Because of the Méring effects shown in Figure 4, if $P_{cv} \leq 0.5$, W_{cv} is slightly underestimated with decreasing P_0. If $P_{cv} > 0.5$, W_{cv} is slightly overestimated with decreasing P_0.

A stronger discrepancy between P_{cv} and $\overline{W}_{cv}$ was observed for tv-cv illites with $P_{cv} \leq 0.2$, $P_0 < 0.8$, and $P_{60} = 0$. These results again reflect the influence of the $2M_1$ structural fragments on the positions of the $11\bar{2}_{tv}$ and 112_{tv} reflections (Fig. 3). In the limiting case in which $P_{cv} = 0$, a decrease in P_0 leads to the migration of the $11\bar{2}_{tv}$ and 112_{tv} reflections away from the $11\bar{2}_{cv}$ and 112_{cv} reflections, respectively, and toward the 023_{2M_1} and 025_{2M_1} reflections. For this reason $\overline{W}_{cv}$ values are negative for tv-$1M$ illites with $P_0 \leq 0.8$ (Table 6). In the other limiting case in which $P_{cv} = 1$, decreases in P_0 lead to migration of the $11\bar{2}_{cv}$ and 112_{cv} reflections away from the $11\bar{2}_{tv}$ and 112_{tv} reflections, respectively, and toward the $11\bar{4}_{2M_1}$ and 114_{2M_1} reflections. For this reason $\overline{W}_{cv}$ exceeds 1.0 for cv-$1M$ illites with $P_0 \leq 0.8$ (Table 6). Thus, if a negative

TABLE 6. W_{cv} values for tv-cv illites containing $n \cdot 120°$ ($P_{60} = 0$) and $n \cdot 60°$ ($P_{60} = 1$) layer rotations, calculated using Equation 4 and the indicated $d(hkl)$ reflection pairs

P_{cv}	P_0	W_{cv} $111, 11\bar{3}$ $P_{60} = 0$	W_{cv} $112, 11\bar{3}$ $P_{60} = 0$	W_{cv} $11\bar{2}, 112$ $P_{60} = 0$	$\overline{W}_{cv}$ $P_{60} = 0$	W_{cv} $111, 11\bar{3}$ $P_{60} = 1$	W_{cv} $112, 11\bar{3}$ $P_{60} = 1$	W_{cv} $11\bar{2}, 112$ $P_{60} = 1$	$\overline{W}_{cv}$ $P_{60} = 1$
0	0.8	—	—	−0.06	−0.06	—	—	−0.05	−0.05
0	0.6	—	—	−0.17	−0.17	—	—	−0.09	−0.09
0	0.5	—	—	—	—	—	—	−0.09	−0.09
0.2	0.8	—	0.13	0.14	0.14	—	0.16	0.15	0.15
0.2	0.6	—	—	0.05	0.05	—	—	0.12	0.12
0.2	0.5	—	—	—	—	—	—	0.09	0.09
0.3	0.8	—	0.26	0.23	0.24	—	0.29	0.25	0.27
0.3	0.6	—	—	0.17	0.17	—	—	0.19	0.19
0.3	0.5	—	—	—	—	—	—	0.19	0.19
0.4	0.8	—	0.37	0.33	0.35	—	0.38	0.32	0.35
0.4	0.6	—	—	0.31	0.31	—	0.28	0.32	0.30
0.4	0.5	—	—	—	—	—	—	0.29	0.29
0.5	0.8	0.53	0.46	0.38	0.46	0.58	0.45	0.37	0.47
0.5	0.6	—	—	0.40	0.40	0.41	0.43	0.41	0.42
0.5	0.5	—	—	—	—	—	0.34	0.42	0.38
0.6	0.8	0.63	0.58	0.54	0.58	0.71	0.59	0.52	0.61
0.6	0.6	—	—	0.58	0.58	0.59	0.56	0.54	0.56
0.6	0.5	—	—	—	—	0.48	0.52	0.57	0.52
0.8	0.8	0.86	0.85	0.80	0.83	0.87	0.81	0.77	0.82
0.8	0.6	0.69	0.82	1.00	0.84	0.83	0.80	0.80	0.81
0.8	0.5	—	—	—	—	0.71	0.83	0.87	0.80
1.0	0.8	1.04	1.04	1.03	1.04	1.05	1.01	0.97	1.01
1.0	0.6	1.06	—	—	1.06	1.03	1.04	1.14	1.07
1.0	0.5	—	—	—	—	1.01	1.13	1.35	1.16

TABLE 7. I/S structural parameters determined by McCarty and Reynolds (1995)

Sample	Bentonite bed and location	Exp%	R*	P_0	P_{cv}	P_{60}
55	Ordovician Ottawa	13	2.5	70	60	40
16	Millbrig, GA	14	3	85	55	60
26	Nasset Ord., IA	15	3	75	35	95
24	Millbrig, KY	26	1	60	60	65
53	Ordovician, WI	19	1.5	65	45	75
39	Deicke, MN	26	1	60	60	45
41	Millbrig, AL	11	3	70	55	60
34	Tioga, NY	10	3	60	80	35
21	Ordovician, KY	15	2.5	75	50	75
8	Deicke, WV	11	3	80	60	30
27	Ordovician, NY	18	1.5	62	75	45
17	Deicke, GA	9	3	65	40	90
15	Ordovician, NY	18	1	60	65	40
7	Ordovician, PA	11	3	70	82	30
42	Ordovician, NY	19	2.5	55	85	30
45	Tioga, NY	13	3	50	98	20
56	Ordovician Ottawa	21	2.5	50	95	35

Note: P_{cv} is the proportion of cv layers used by McCarty and Reynolds (1995) to model their experimental diffraction patterns with WILDFIRE.
* R = Reichweite.

TABLE 8. P_{cv} and $\overline{W}_{cv}$ calculated from the simulated (WILDFIRE) and experimental diffraction patterns from McCarty and Reynolds (1995)

Sample	P_{cv}	$\overline{W}_{cv}$ $T_{tv} = 0.383$ $T_{cv} = 0.308$	$P_{cv} - \overline{W}_{cv}$	$\overline{W}_{cv}^{exp}$ $T_{tv} = 0.383$ $T_{cv} = 0.308$	$\overline{W}_{cv}^{exp}$ $T_{tv} = 0.40$ $T_{cv} = 0.30$
55	60	58	2	57	59
16	55	53	2	46	51
26	35	27	8	22	34
24	60	51	9	66	65
53	45	37	8	32	41
39	60	45	15	65	66
41	55	53	2	45	49
34	80	77	3	72	72
21	50	47	3	47	41
8	60	63	3	38	46
27	75	71	4	52	56
17	40	30	10	8	23
15	65	61	4	33	42
7	82	85	3	52	56
42	85	76	9	42	49
45	98	79	19	70	70
56	95	79	16	53	56

Note: $\overline{W}_{cv}$ calculated from experimental and simulated XRD patterns using T_{ef} (Eq. 3), where $T_{tv} = 0.383$ and $T_{cv} = 0.308$, in comparison with W_{cv} calculated from experimental patterns using Equation 4, where $T_{tv} = 0.40$ and $T_{cv} = 0.30$.

W_{cv} value is obtained using Equation 4, it means there are no, or only a few, cv layers, but there are rotational stacking faults; and if $W_{cv} > 1$, there are no, or only a few, tv layers, but the structure contains rotational stacking faults.

Determination of W_{cv} values for I/S samples

The techniques described here were tested on natural illite-smectite samples studied by McCarty and Reynolds (1995), who compared simulated XRD patterns with experimental ones to determine the proportion of tv and cv layers and the amount and type of layer rotations. The sample designations, I/S expandability, cv-layer content, and type and amount of rotational disorder obtained from the model XRD patterns by McCarty and Reynolds (1995) are shown in Table 7. The authors assumed that $T_{tv} = 0.383$ and $T_{cv} = 0.308$. We used the $d(111)$, $d(11\bar{2})$, $d(112)$, and $d(11\bar{3})$ values obtained from their experimental and simulated XRD patterns to determine the W_{cv} values using Equations 4 and 2, respectively (Table 8).

The second column of Table 8 contains proportions of cv 2:1 layers, P_{cv}, determined by McCarty and Reynolds (1995). The next column contains proportions of cv 2:1 layers calculated using Equation 4. The T_{ef} values were determined using Equation 3 and the spacings of the $11l$ and $11\bar{l}$ reflections calculated from the simulated XRD patterns. Comparison of P_{cv} and W_{cv} permits us to estimate errors resulting from the presence of different types of stacking faults and peak broadening from small particle size (small CSD) because all other parameters, including T_{tv} and T_{cv}, were known a priori. As seen in Table 8 the differences between P_{cv} and W_{cv} for the samples under study usually do not exceed 10%. Samples 17 and 16 are exceptions, although even for these samples relative errors do not exceed 20%. The XRD patterns from these two samples contain only two broad and weak maxima with 111 and 113 indices; that is, the samples are characterized by very high proportions of rotational stacking faults ($P_0 = 50\%$) and few tv 2:1 layers ($W_{cv} = 90$–100%). In general we conclude that the agreement between P_{cv} and W_{cv} is quite satisfactory. This is an important conclusion because the XRD patterns were simulated for the models with a wide interval of values for variable parameters, including $0.5 \leq P_0 \leq 1.0$ and expandability from 9 to 30% (McCarty and Reynolds 1995).

Equations 3 and 4 were applied to both experimental and simulated diffraction patterns. W_{cv}^{exp} results from applying these equations to the experimental diffraction patterns obtained by McCarty and Reynolds (1995), and W_{cv}^{w} results from using Equation 3 or 4 on calculated WILDFIRE diffraction patterns. The fifth column of Table 8 contains proportions of cv 2:1 layers, W_{cv}^{exp}, determined using Equation 4, assuming that $T_{tv} = 0.383$ and $T_{cv} = 0.308$. The T_{ef} values were obtained from Equation 3 using values of $d(11l)_{exp}$ and $d(11\bar{l})_{exp}$ calculated from the experimental XRD patterns. At first glance it appears that there is significant disagreement between W_{cv}^{w} determined using Equations 3 and 4 on the WILDFIRE patterns and W_{cv}^{exp}, obtained using the same procedure, which is rather surprising. However, further analysis of the data obtained by McCarty and Reynolds (1995) shows that $d(11l)$ and $d(11\bar{l})$ values calculated from the experimental and simulated XRD patterns corresponding to the same sample are characterized by a systematic deviation, where $d(11\bar{l})_{exp} > d(11\bar{l})_{calc}$ and $d(11l)_{exp} < d(11l)_{calc}$ (see Table 5; McCarty and Reynolds 1995). It should be emphasized that the difference between d_{calc} and d_{exp}, which corresponds to reflections with the same $11l$ indices, exceeds experimental errors in determination of the spacing values. To illustrate let us compare $d(11l,11\bar{l})_{calc}$ and $d(11l,11\bar{l})_{exp}$ for sample 13 (McCarty and Reynolds 1995).

The spacings of the 111, 11$\bar{2}$, 112, and 11$\bar{3}$ reflections calculated from the simulated and experimental XRD patterns were equal, respectively, to 3.883 and 3.859 Å, 3.611 and 3.632 Å, 3.122 and 3.096 Å, and 2.896 and 2.906 Å: This means that the unit-cell parameters and, in particular, the T_{tv} and T_{cv} values that were used for the calculations do not correspond precisely to those of the samples under study. Moreover, comparison of the experimental and calculated XRD patterns was confined by semiquantitative fitting, and at least for samples with high proportions of stacking faults (P_0 = 0.6–0.5), the precision in the determination of the proportion of cv layers by simulation of XRD patterns may be overestimated.

Taking into account these considerations, we assumed that the actual structures of the samples under study are characterized by T_{tv} and T_{cv} values that differ from those used by McCarty and Reynolds (1995). In fact, Drits et al. (1993) showed that T_{tv} = 0.400 and T_{cv} = 0.302 for pure tv-1*M* and cv-1*M* illites, respectively. Unfortunately, the WILDFIRE program permits calculations of XRD patterns with interstratification of only the unit-cell parameters for pure tv-1*M* and cv-1*M* illites. For this reason we cannot simulate XRD patterns with new unit-cell parameters. The use of T_{tv} = 0.40 and T_{cv} = 0.30 values may improve the agreement between W_{cv}^{exp} and W_{cv}^{w}, but more work is needed to confirm this possibility.

The essential discrepancies hold again for samples with the lowest degree of structural ordering and the highest values of W_{cv}, 0.8–0.9 (samples 17, P_0 = 0.5; sample 15, P_0 = 0.55; sample 16, P_0 = 0.5). We conclude that the technique cannot be applied if the XRD pattern of a sample contains only 111 and 11$\bar{3}$ reflections, which is the case with sample 56. However, the presence of only these two peaks means that the sample is dominated by rotational stacking faults and cv layers (>75%).

Let us consider now the results of the determination of W_{cv} for the samples under study using our version of Méring's approach. To use Equation 2, one must know the $d(11l,11\bar{l})_{tv}$ and $d(11l,11\bar{l})_{cv}$ values. To determine these we used the values of *a*, *b*, and *c* sin β used by McCarty and Reynolds (1995) for pure tv-1*M* and cv-1*M* illites (*a* = 5.199, *b* = 9.005, *c* sin β = 9.98 Å). However, the values of the β angles, 101.77 and 98.88° for the tv-1*M* and cv-1*M* structures, respectively, were different. These β_{tv} and β_{cv} values lead to T_{tv} = 0.400 and T_{cv} = 0.300, respectively. For these unit-cell parameters for tv-1*M* and cv-1*M* illites, Equation 2 for $(11l,11\bar{l})_{obs}$ reflections can be written as follows: $W_{cv} = 50.44 - 192.0/d_{111_{obs}}$; $W_{cv} = 189.4/d_{11\bar{2}_{obs}} - 57.87$; $W_{cv} = 40.69 - 124.3/d_{112_{obs}}$; $W_{cv} = 155.1/d_{11\bar{3}_{obs}} - 53.10$. Table 9 contains P_{cv} values determined by McCarty and Reynolds (1995) and $\overline{W}_{cv}$ values calculated using experimental values of $d(111)_{exp}$, $d(11\bar{2})_{exp}$, $d(112)_{exp}$, and $d(11\bar{3})_{exp}$. As shown in the previous section, the good agreement between P_{cv} and W_{cv} was achieved when only $d(112)$ values were used. For this reason Table 9 also contains W_{cv} values calculated using Equation 2 and the experimental spacings for 112_{exp} reflections.

TABLE 9. P_{cv} and $\overline{W}_{cv}$ calculated from WILDFIRE and experimental diffraction patterns obtained by McCarty and Reynolds (1995)

Sample	P_{cv}	$\overline{W}_{cv}^{exp}$	W_{cv} $d(112)$ only	$P_{cv} - \overline{W}_{cv}^{exp}$
55	60	63	68	3
16	55	56	47	1
26	35	30	47	5
24	60	54	81	6
53	45	39	54	6
39	60	69	—	9
41	55	62	47	7
34	80	79	87	1
21	50	39	54	11
8	60	52	54	8
27	75	61	68	14
17	40	27	28	13
15	65	45	54	20
7	82	64	68	18
45	98	76	—	22
42	85	69	—	16
56	95	72	—	23

Note: $\overline{W}_{cv}$ values are from Equation 2 and the available $d(111)_{exp}$, $d(11\bar{2})_{exp}$, $d(112)_{exp}$, and $d(11\bar{3})_{exp}$ reflections, in comparison with the W_{cv} values calculated using Equation 2 and only the $d(112)_{exp}$ reflection.

Taking into account the uncertainty in the precision of the W_{cv}^{w} value determination and the high content of rotational stacking faults in the samples under study, the agreement between W_{cv}^{w} and W_{cv}, obtained using the technique proposed, is very good (Table 9). For most samples the relative discrepancy $[(P_{cv} - \overline{W}_{cv})/P_{cv}]$ does not exceed 0.22. For only two samples (15 and 17) is this value equal to 0.30. As expected, the use of single $d(112)_{obs}$ values also led to good agreement between P_{cv} and W_{cv}^{exp} (Table 9).

Let us consider another example, which illustrates the effectiveness of the techniques proposed, from a study of the mechanism of the structural transformation of illites in samples from Dovna Ves hydrothermal deposits (Drits et al. 1996). First note that one of the problems in XRD studies of I/S is that most I/S samples have a low degree of structural ordering. Drits et al. (1996) proposed a technique for artificially increasing the three-dimensional order of I/S. To do this they saturated samples with K, subjected them to 60 cycles of wetting and drying, and heated them at 300 °C for 2 h. The XRD patterns from the treated I/S samples resulted in strong 11*l* and 02*l* diffraction maxima. These authors also developed a computer program to decompose XRD patterns for individual diffraction maxima. This procedure increased the precision in determination of the $d(11l,11\bar{l})_{obs}$ and T_{ef} values. It was shown that the T_{ef} values varied from 0.30 to 0.39 for samples with the highest (W_s = 50%) and lowest (W_s = 6%) expandabilities, respectively. Application of the proposed techniques to the Dovna Ves hydrothermal I/S samples showed that their structural transformations were accompanied not only by variations in the proportion of illite and smectite layers and the pattern of their alternation but also by a change in the proportion of cv and tv 2:1 layers. In particular, an increase of illite layers and K content was accompanied by increasing tv 2:1 layers

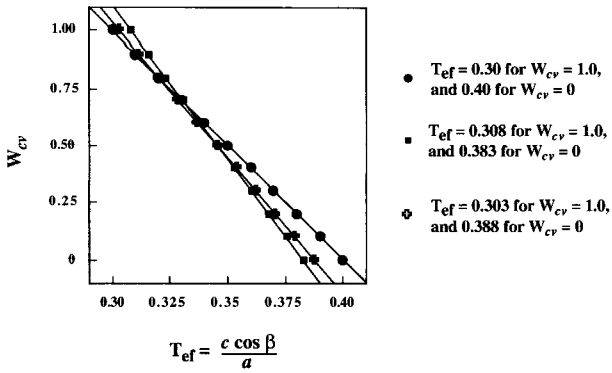

FIGURE 8. The dependence between T_{ef} and W_{cv} calculated using Equation 4, where T_{tv} = 0.40, T_{cv} = 0.30, T_{tv} = 0.383, T_{cv} = 0.308 and T_{tv} = 0.388, T_{cv} = 0.303.

from 0 to 90%. These authors also found that T_{tv} = 0.40 and T_{cv} = 0.30.

CONCLUSIONS

The diffraction effects observed in random powder preparations of 1*M* and 1*Md* illites and I/S with a range of expandabilities, cv-tv layer content, and $n \cdot 60°$ and $n \cdot 120°$ rotational disorder are explained using Méring's principles. Samples with significant $n \cdot 60°$ disorder have $2M_2$ polytype coherent-scattering domains (CSDs), and when rotational disorder is $n \cdot 120°$ there are $2M_1$ CSDs, both of which contribute to diffraction effects in the 1*Md* category.

Two new techniques have been proposed for semi-quantitative determination of cv-tv layer-type proportions. Errors in the determination of W_{cv} depend on the total content of cv layers and on the degree of the structural perfection of the sample. The results obtained for natural I/S samples show that the level of accuracy in the determination of W_{cv}^{exp} achieved by the Méring approach is similar to that provided by the simulation of XRD patterns using the WILDFIRE program.

The utilization of Equations 2 and 4 requires caution, however, especially if the I/S samples have a high degree of rotational disorder and thin CSDs. The XRD patterns from such samples usually contain broad and weak 11*l* reflections. Moreover, some of them contain only two very broad maxima that have 111 and $11\bar{3}$ indices. Precise determination of the peak position by conventional techniques is not always possible. An artificial increase in the three-dimensional ordering of I/S samples by K saturation and application of decomposition of XRD patterns for individual maxima may increase the reliability of the results obtained (Drits et al. 1996). Reliable results are obtained when a mean of W_{cv} values calculated for all obtained ($11l$,$11\bar{l}$) reflections is determined. Our experience has also shown that nearly the same agreement is achieved between actual cv layer content and W_{cv} calculated by Equation 2 using only $d(112)$ reflections because these maxima are not very sensitive to the type and content of stacking faults.

Let us note some advantages of the application of Equations 3 and 4. First, the mean T_{ef} values are not very sensitive to CSD thickness, the degree of structural perfection, and variation in the chemical composition of illites. Second, variations in the T_{tv} and T_{cv} values do not strongly influence the calculated W_{cv} values, especially when $0.8 > W_{cv} > 0.2$. For example, Figure 8 shows the dependence between T_{ef} and W_{cv} calculated using Equation 4 when T_{tv} = 0.383, T_{cv} = 0.308 and T_{tv} = 0.40, T_{cv} = 0.30. The relatively low sensitivity of W_{cv} to variation in T_{tv} and T_{cv} may have significance if these values depend, for example, on the chemical composition of illites. According to published data (Bailey 1984; Drits et al. 1993; Zvyagin et al. 1985), T_{tv} = 0.40 and T_{cv} = 0.30 for Fe-free tv-1*M* and cv-1*M*, respectively. However, Sakharov et al. (1990) found T_{tv} = 0.384 for an Fe-bearing illite sample with the structural formula $K_{0.74}Na_{0.07}Ca_{0.06}$-$(Al_{1.11}Fe^{3+}_{0.34}Fe^{2+}_{0.21}Mg_{0.42})(Si_{3.48}Al_{0.52})O_{10}(OH)_2$ and *b* angle = 9.038 Å. One caveat in using Equation 3: The cv 111 reflection should not be used to determine W_{cv} if the sample under study has more than about 20% expandable smectite layers unless the sample is treated by the method proposed by Drits et al. (1996). This peak migrates markedly with increasing expandability (Reynolds, personal communication).

At present there are only a few publications describing the coexistence of tv and cv 2:1 layers within a sample structure. The techniques described here may help to reveal a diversity of illite and I/S samples relating to the conditions of their formation and transformation.

ACKNOWLEDGMENTS

V.A.D. thanks the International Science Foundation established by George Soros for the support of this work. Both authors thank Dennis Eberl and the U.S. Geological Survey, Water Resources Division, for help and support. We also thank R.C. Reynolds for his remarks, the opportunity to use the computer program WILDFIRE, and his careful review of the manuscript. The paper was improved enormously by Reynolds's efforts and expertise. Equal gratitude goes to J. Walker for his painstaking reviews of the original and a later version of this paper. Thanks also go to Gene Whitney, who helped to improve this work.

REFERENCES CITED

Bailey, S.W. (1984) Crystal chemistry of the true micas. In Mineralogical Society of America Reviews in Mineralogy, 13, 13–60.

Drits, V.A., and Sakharov, B.A. (1976) X-ray structural analysis of interstratified minerals, 256 p. Naua, Moscow (in Russian).

Drits, V.A., PlanÇon, B.A., Sakharov, B.A., Besson, G., Tsipursky, S.I., and Tchoubar, C. (1984) Diffraction effects calculated for structural models of K-saturated montmorillonite containing different types of defects. Clay Minerals, 19, 541–561.

Drits, V.A., Weber, F., Salyn, A.L., and Tsipursky, S.I. (1993) X-ray identification of one-layer illite varieties: Application to the study of illites around uranium deposits of Canada. Clays and Clay Minerals, 41, 389–398.

Drits, V.A., Salyn, A.L., and Sucha, V. (1996) Structural transformation of illite-smectites from Dolná Ves hydrothermal deposit: Dynamics and mechanisms. Clays and Clay Minerals, 44(2), 181–190.

Gavrilov, Y.O., and Tsipursky, S.I. (1987) Clay minerals from low- and middle-Jurassic deposits of different structural and facial zones of the central Caucasus. Lithology and Raw Materials, 6, 57–72 (in Russian).

Horton, D. (1983) Argillitic alteration associated with the amethyst vein

system, Creede Mining District, Colorado. Ph.D. dissertation, University of Illinois, Urbana-Champaign.

McCarty, D.K., and Reynolds, R.C. (1995) Rotationally disordered illite-smectite in Paleozoic K-bentonites. Clays and Clay Minerals, 43, 271–284.

Méring, J. (1949) L'Interférence des rayons X dans les systems à stratification désordonnée. Acta Crystallographica, 2, 371–377.

Reynolds, R.C. (1980) Interstratified clay minerals. In G.W. Brindley and G. Brown, Eds., Crystal structures of clay minerals and their X-ray identification, p. 249–303. Mineralogical Society, London, U.K.

Reynolds, R.C., and Hower, J. (1970) The nature of interlayering in mixed-layer illite-montmorillonite. Clays and Clay Minerals, 18, 25–36.

Reynolds, R.C., Jr. (1993) Three-dimensional powder X-ray diffraction from disordered illite: Simulation and interpretation of the diffraction patterns. In R.C. Reynolds, Jr. and J.R. Walker, Eds., Clay minerals society workshop lectures, vol. 5: Computer applications to X-ray powder diffraction analysis of clay minerals, p. 43–77. The Clay Minerals Society, Boulder, Colorado.

Reynolds, R.C., Jr., and Thomson, C.H. (1993) Illite from the Potsdam Sandstone of New York: A probable noncentrosymmetric mica structure. Clays and Clay Minerals, 41, 66–72.

Sakharov, B.A., Besson, G., Drits, V.A., Kamenava, M.Yu, Salyn, A.L., and Smoliar, B.B. (1990) X-ray study of the nature of stacking faults in the structure of glauconites. Clay Minerals, 25, 419–435.

Środoń, J., and Eberl, D.D. (1984) Illite. In Mineralogical Society of America Reviews in Mineralogy, 13, 495–544.

Tsipursky, S.I., and Drits, V.A. (1984) The distribution of octahedral cations in the 2:1 layers of dioctahedral smectites studied by oblique-texture electron diffraction. Clay Minerals, 19, 177–193.

Zvyagin, B.B., Rabotnov, V.T., Sidorenko, O.V., and Kotelnikov, D.D. (1985) Unique mica from noncentrosymmetric layers. Izvestia Akademie Nauk SSSR, Seriya Geologicheskaya, 35, 121–124 (in Russian).

Manuscript received August 10, 1995
Manuscript accepted April 1, 1996